Hindawi
Shock and Vibration
Volume 2019, Article ID 4609754, 8 pages
https://doi.org/10.1155/2019/4609754

Research Article

Modeling and Simulation of Energy-Regenerative Active Suspension Based on BP Neural Network PID Control

Jiang Liu, Xinjun Li, Xilong Zhang, and Xiufeng Chen

School of Mechanical and Automotive Engineering, Qingdao University of Technology, Qingdao 266520, China

Correspondence should be addressed to Jiang Liu; liujiang@qut.edu.cn

Received 18 April 2019; Accepted 3 June 2019; Published 18 June 2019

Academic Editor: Angelo Marcelo Tusset

In this paper, an electromagnetic energy-regenerative suspension system is proposed to achieve active control and vibration energy harvesting. For this system, a PID controller based on BP neural network algorithm is designed and vehicle dynamic performances are studied. Based on the traditional energy-regenerative efficiency calculation, a novel self-supply energy efficiency concept is proposed to evaluate the utilization effect of the recycled energy for this dual-functional suspension. Simulations are carried out, and the results show that the vehicle dynamic performances are effectively improved under different input conditions, including road surfaces and vehicle speeds. Furthermore, the energy-regenerative suspension can recover part of vibration energy, where the self-supply energy efficiency is about 55% and the energy-regenerative efficiency is about 16%. Meanwhile, the BP-PID algorithm also enables the suspension system's self-adaptability and stability characteristics on its energy recovery capability.

1. Introduction

Due to the limitation of the passive suspension, the handing stability and ride comfort of the vehicle cannot be satisfied at the same time. Therefore, the research and application of the active suspension is becoming increasingly popular, which effectively improves the vehicle dynamic performance [1–3]. However, the active suspension adds a new problem in terms of vehicle energy consumption while improving its vibration response. Therefore, many scholars have begun to study the energy-regenerative active suspension. By recovering the dissipated vibration energy and storing it for the active control of suspension, the energy-regenerative active suspension can effectively improve the energy utilization and reduce the energy loss at the same time [4–6]. Compared with mechanical energy-regenerative suspension, the electromagnetic energy-regenerative suspension has faster response and higher energy recovery efficiency, so it has become the hotspot of research studies [7–9].

Okada et al. [10, 11] proposed an electromagnetic energy regeneration system, in which a linear DC motor is used as an actuator, and a bidirectional voltage charging circuit is used to harvest the electric energy generated by the high-speed movement of the actuator and charge the battery. But when the system moves at a low speed, the actuator cannot charge the battery and provide enough power. Suda et al. [12] developed a prototype of the electromagnetic damper, which is composed of a rotating DC motor and a ball screw mechanism. Later, they improved the suspension by adding a planetary gear mechanism. Nakano et al. [13] proposed a self-powered active vibration isolation control system that uses a linear DC motor actuator to achieve the vibration control and the energy regeneration. Martins et al. [14] compared the layouts of the hydraulic and electromagnetic active suspension, calculated the actuator requirements, and proved the feasibility of electromagnetic suspension in application. Li et al. [15, 16] designed a retrofit regenerative shock absorber based on a permanent magnetic generator and a rack-pinion mechanism and performed bench experiments and road tests for validation.

Most of the references mentioned above achieve the optimization of energy-regenerative suspension from the structure. However, it turns out that the control algorithm has a significant influence on the energy-regenerative efficiency [17, 18]. Due to its strong self-learning and self-

adaptive ability, the neural network algorithm has been widely used in the field of nonlinear control. As a mature neural network algorithm, the BP neural network is often used for the optimization of suspension control [19], but it has the risk of slow convergence rate and is easy to fall into local minimization. Therefore, some researchers combine the BP neural network with other control algorithm to solve these problems. Liu and Hu [20] proposed a PSO-BP algorithm to optimize the vehicle suspension, which improves the slow convergence rate and poor global convergence of traditional BP algorithm and significantly improves the suspension performances. Zhu et al. [21] proposed a GA-BP algorithm to identify road surfaces in the mining field. Compared with the standard BP algorithm, the truck's ride comfort is improved obviously through simulations and road tests. Owing to its simple structure and good real-time performance, PID controller has been widely used in the active control of suspensions [22–24], but none of previous studies combine BP neural network with PID controller to solve energy regeneration and active control for suspensions.

This paper proposes a new electromagnetic energy-regenerative active suspension (EERAS) system for both active control and energy recovery. Besides the improvement of the vehicle dynamic performance as what the traditional suspension control studies have achieved, the new system can recover the vibration energy from the suspension working space simultaneously, which is conducive to saving energy and increasing mileage. The suspension actuator consists of a ball screw energy-regenerative shock absorber and a permanent magnet brushless DC motor. The controller is designed based on BP-PID algorithm. The control effects and the energy-regenerative effects are analyzed through simulations, which are performed under different road surfaces or vehicle speeds. The paper is organized as follows.

In Section 2, the model of EERAS system is established, including the quarter-car model and the control circuit model. In addition, a novel concept is proposed to measure the utilization efficiency of the recovered energy. In Section 3, a controller based on BP-PID algorithm is designed for the suspension control. In Section 4, the simulations are carried out under different input conditions to verify the improvement of the suspension performances and the ability to recover vibration energy of the suspension. The main conclusions are drawn in Section 5.

2. Model of the EERAS System

2.1. Structure of the EERAS System. The structure of the EERAS system is shown in Figure 1. It is mainly composed of a spring, a ball screw actuator, a controller, a charging circuit, batteries and corresponding sensors, and so on. During the running of the vehicle, the energy-regenerative device extends and compresses with the uneven road surface. The screw shaft moves up and down to make the ball nut rotate. The nut is connected to the motor through the gear set to increase rotation. The motor works in the power generation or braking state according to the controller's instructions so as to actively attenuate and harvest the body vibration. The recovered energy will be stored in the batteries through the charging circuit.

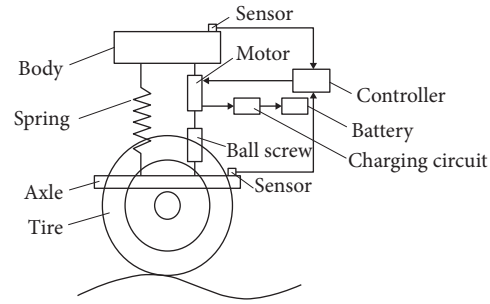

Figure 1: Structure of the EERAS system.

2.2. Control Principle of the EERAS System. Based on a 2-DOF quarter-car model, we apply the BP-PID control algorithm to the electromagnetic energy-regenerative active suspension. And a PI controller is added to ensure the consistency between the actual force and the desired force. The control principle is shown in Figure 2. For this system, the BP-PID controller aims at reducing body acceleration to improve vehicle ride comfort, so we define y as the body acceleration, one of the 2-DOF quarter-car model's output parameters. r is the body acceleration with a desired value of 0. e is the deviation between the desired value and actual value, which is taken as the input of the BP-PID controller. Then, the BP-PID controller offers a desired force to the PI controller, and the control circuit outputs actual force to the quarter-car model. φ is the constant of the screw motor, which is used to convert the desired force into the desired current.

2.3. Quarter-Car Model. A 2-DOF quarter-car model is established to analyze the suspension dynamic characteristics, as shown in Figure 3. In the model, m_b and m_w are the sprung mass and unsprung mass; x_b and x_w are the displacement of the sprung mass and unsprung mass; x_g is the road displacement; K_s is the suspension stiffness; K_t is the tire stiffness; C_s is the inherent damper coefficient of the system; and F is the actuator control force.

The dynamic differential equations of the model are

$$\begin{aligned} m_b\ddot{x}_b &= K_s\left(x_w - x_b\right) + C_s\left(\dot{x}_w - \dot{x}_b\right) + F, \\ m_w\ddot{x}_w &= K_t\left(x_g - x_w\right) - K_s\left(x_w - x_b\right) - C_s\left(\dot{x}_w - \dot{x}_b\right) - F. \end{aligned} \tag{1}$$

2.4. Random Road Model. When analyzing the dynamic characteristics of the suspension system, the random road model is an important part. In this paper, a filtering white noise is used to describe the random road input,

$$\dot{x}_g(t) = -2\pi f_0 x_g(t) + 2\pi\sqrt{G_0 v_0}\, w(t), \tag{2}$$

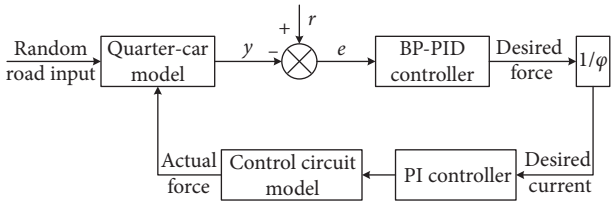

Figure 2: BP-PID control schematic of the EERAS system.

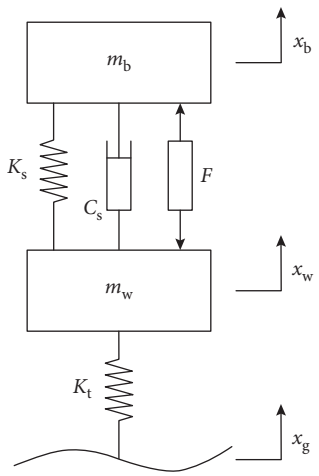

Figure 3: 2-DOF quarter-car model.

where f_0 is the lower cutoff frequency and set as 0.1 Hz; G_0 is the road roughness coefficient; v_0 is the forward vehicle speed; and w is the Gaussian white noise expected to be zero in mathematics.

2.5. Control Circuit Model. The circuit schematic diagram is shown in Figure 4, where U is the power supply voltage; I is the armature loop current; R is the armature loop internal resistance; M is the DC motor; and L is the inductance.

For an ideal actuator, it has the following characteristics [15]:

$$E_M = \varphi \dot{z}, \tag{3}$$

$$F = \varphi I, \tag{4}$$

where E_M is the electromotive force of the motor; φ is the constant of the screw motor, $\varphi = k/d$, k is the motor constant and d is the screw lead; and $\dot{z}$ is the axial speed of the ball screw.

The circuit equation can be obtained as follows from Figure 4:

$$U = L\frac{dI}{dt} + RI + E_M. \tag{5}$$

According to equations (4) and (5), we can learn that when the screw's motor constant is unchanged, the active control force is positively correlated with the armature loop current. And by adjusting the power supply voltage, the armature loop current can be changed; then, the active control force is adjusted.

The control circuit takes the deviation value of the armature current as the input signal:

$$\begin{aligned} I_0 &= \frac{F_0}{\varphi}, \\ e &= I_0 - I, \end{aligned} \tag{6}$$

where I_0 is the ideal armature loop current; F_0 is the ideal active control force; and e is the deviation between the ideal current and the actual current.

The PI control voltage formula is as follows:

$$U = K_p e + K_i \int_0^t e\, dt, \tag{7}$$

where K_p and K_i are the proportional coefficient and integral coefficient of the PI controller, respectively.

Substituting equations (3) and (7) into equation (5), we can get

$$K_p e + K_i \int_0^t e\, dt - \varphi \dot{z} = L\frac{dI}{dt} + RI. \tag{8}$$

Performing a Laplace transform on equation (8), we can get

$$I(s) = \left[\left(K_p + \frac{K_i}{s}\right)e(s) - \varphi z(s)s\right] \cdot \frac{1}{Ls + R}, \tag{9}$$

where s is a Laplacian operator.

Figure 5 is a schematic diagram of the PI controller.

2.6. Self-Supply Energy Efficiency. P_r is the power of the suspension to recover energy, and P_c is the power of the suspension to consume energy. The ratio between P_r and P_c is defined as the self-supply energy efficiency, representing the energy utilization effect of the suspension as follows:

$$\eta = \frac{P_r}{P_c}. \tag{10}$$

When the motor functions as a generator, it can be obtained from Figure 4(a) that

$$U_D = E_M - U_R, \tag{11}$$

where U_D is the power supply voltage in the generator state and U_R is the voltage of the internal resistance.

Substituting equations (3) and (4) into equation (11), we can get

$$U_D = \varphi \dot{z} - IR = \varphi \dot{z} - \frac{FR}{\varphi}. \tag{12}$$

Therefore, the power of the motor to recover energy is

$$P_r = U_D \cdot I = \varphi \dot{z} \cdot I - \frac{FR}{\varphi} \cdot I = F\dot{z} - \frac{F^2 R}{\varphi^2}. \tag{13}$$

Similarly, we can get the power supply voltage U_E and the power P_c of the suspension to consume energy in the motor state, as follows:

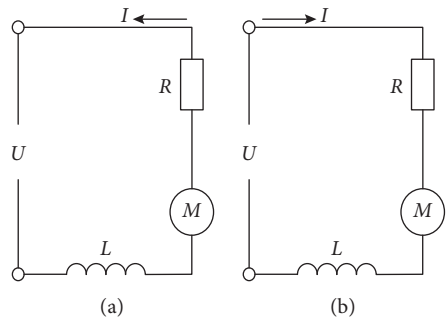

Figure 4: Schematic of the control circuit model. (a) Generator. (b) Motor.

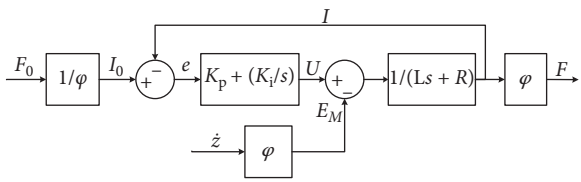

Figure 5: PI controller.

$$U_E = E_M + U_R = \varphi\dot{z} + IR = \varphi\dot{z} + \frac{FR}{\varphi}, \tag{14}$$

$$P_c = U_E \cdot I = \varphi\dot{z} \cdot I + \frac{FR}{\varphi} \cdot I = F\dot{z} + \frac{F^2R}{\varphi^2}. \tag{15}$$

Substituting equations (13) and (15) into equation (10), we can get

$$\eta = \frac{P_r}{P_c} = \frac{F\dot{z} - F^2R/\varphi^2}{F\dot{z} + F^2R/\varphi^2} = 1 - \frac{2F^2R/\varphi^2}{F\dot{z} + F^2R/\varphi^2} = 1 - \frac{2}{1 + \varphi^2\dot{z}/RF}$$
$$= 1 - \frac{2}{1 + E_M/U_R}. \tag{16}$$

2.7. Energy-Regenerative Efficiency. The power P_d of the thermal energy dissipated by the passive suspension damper is written as follows:

$$P_d = \frac{1}{2}C\dot{z}^2, \tag{17}$$

where C is the damping of the passive suspension damper.

The energy-regenerative efficiency η_s is defined as the ratio between P_r and P_d, representing the suspension energy recovery effect; then, we can get

$$\eta_s = \frac{P_r}{P_d}. \tag{18}$$

3. BP-PID Controller Design

3.1. Principle of BP-PID Controller. A new BP-PID controller is shown in Figure 6. The PID controller performs closed-loop feedback on the controlled object. The BP neural network adjusts the three parameters K_p, K_i, and K_d for the PID controller. The parameters can be adjusted in real time according to the state of the system so as to achieve a better dynamic performance.

3.2. BP-PID Algorithm. We firstly built a three-layer structure for the BP neural network. The number of nodes in the input layer is 4. The input vector is $x = [r(k), y(k), e(k), 1]$, where $r(k)$ is the desired output value of the system, $y(k)$ is the actual output value of the system, and $e(k)$ is the deviation between the expected output and the actual output of the system. For the hidden layer, the number of nodes is 5. And the number of nodes in the output layer is 3, corresponding to the three parameters K_p, K_i, and K_d. Therefore, the structure of this BP neural network is 4-5-3.

The input of the j-th neuron in the input layer is x_j, and the output is

$$O_j^{(1)} = x_j, \quad j = 1, 2, 3, 4. \tag{19}$$

The input of the i-th neuron in the hidden layer is

$$\text{net}_i^{(2)}(k) = \sum_{j=1}^{4} w_{ij}^{(2)} O_j^{(1)} + \theta_i^{(2)}, \quad i = 1, 2, 3, 4, 5, \tag{20}$$

where $w_{ij}^{(2)}$ is the connection weight between the hidden layer neuron i and the input layer neuron j and $\theta_i^{(2)}$ is the threshold of the hidden layer neuron i.

The output of the i-th neuron in the hidden layer is

$$O_i^{(2)} = f\left(\text{net}_i^{(2)}(k)\right), \tag{21}$$

where $f(\cdot)$ is the activation function. It takes the positive and negative symmetric sigmoid function, that is,

$$f(x) = \frac{e^x - e^{-x}}{e^x + e^{-x}}. \tag{22}$$

The input of the l-th neuron in the output layer is

$$\text{net}_l^{(3)}(k) = \sum_{i=1}^{5} w_{li}^{(3)} O_i^{(2)} + \theta_l^{(3)}, \quad l = 1, 2, 3, \tag{23}$$

where $w_{li}^{(3)}$ is the connection weight between the output layer neuron l and the hidden layer neuron i and $\theta_l^{(3)}$ is the threshold of the output layer neuron l.

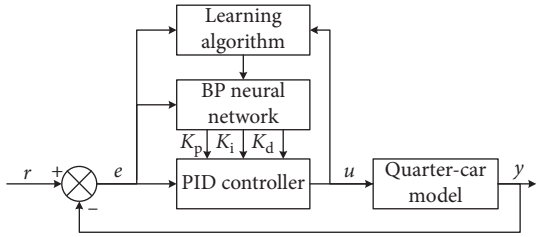

Figure 6: Structural sketch of BP-PID controller.

The output of the l-th neuron in the output layer is

$$O_l^{(3)} = g\left(\text{net}_l^{(3)}(k)\right), \tag{24}$$

where $O_1^{(3)} = K_p, O_2^{(3)} = K_i, O_3^{(3)} = K_d$. Since K_p, K_i, and K_d are always positive, the activation function takes a non-negative sigmoid function, that is,

$$g(x) = \frac{e^x}{e^x + e^{-x}}. \tag{25}$$

The performance index function is as follows:

$$E(k) = \frac{1}{2}(r(k) - y(k))^2. \tag{26}$$

The weight correction of BP neural network adopts the gradient descent method. An inertia term is added, to make the search procedure quickly converge to the global minimum.

$$\Delta w_{li}^{(3)}(k) = -\eta \frac{\partial E(k)}{\partial w_{li}^{(3)}(k)} + \alpha \Delta w_{li}^{(3)}(k-1), \tag{27}$$

where η is the learning rate and α is the inertia coefficient.

$$\frac{\partial E(k)}{\partial w_{li}^{(3)}(k)} = \frac{\partial E(k)}{\partial y(k)} \cdot \frac{\partial y(k)}{\partial u(k)} \cdot \frac{\partial u(k)}{\partial O_l^{(3)}(k)} \cdot \frac{\partial O_l^{(3)}(k)}{\partial \text{net}_l^{(3)}(k)} \cdot \frac{\partial \text{net}_l^{(3)}(k)}{\partial w_{li}^{(3)}(k)},$$

$$\frac{\partial \text{net}_l^{(3)}(k)}{\partial w_{li}^{(3)}(k)} = O_i^{(2)}(k). \tag{28}$$

We substitute the symbolic function $\text{sgn}[\partial y(k)/\partial u(k)]$ for the unknown quantity $\partial y(k)/\partial u(k)$. And the resulting calculation inaccuracy is compensated by adjusting the learning rate η. Therefore, the correction formulas for the weights and thresholds of the output layer are as follows:

$$\begin{aligned} \Delta w_{li}^{(3)}(k) &= \alpha \Delta w_{li}^{(3)}(k-1) + \eta \delta_l^{(3)} O_i^{(2)}(k), \\ \Delta \theta_l^{(3)}(k) &= \alpha \Delta \theta_l^{(3)}(k-1) + \eta \delta_l^{(3)}, \\ \delta_l^{(3)} &= e(k)\text{sgn}\left[\frac{\partial y(k)}{\partial u(k)}\right] \frac{\partial u(k)}{\partial O_l^3(k)} g'\left(\text{net}_l^{(3)}(k)\right), \end{aligned} \tag{29}$$

where $g'(\cdot) = g(x)(1 - g(x))$.

Similarly, we can get the modified formulas for the weights and thresholds of the hidden layer:

$$\begin{aligned} \Delta w_{ij}^{(2)}(k) &= \alpha \Delta w_{ij}^{(2)}(k-1) + \eta \delta_i^{(2)} O_j^{(1)}(k), \\ \Delta \theta_i^{(2)}(k) &= \alpha \Delta \theta_i^{(2)}(k-1) + \eta \delta_i^{(3)}, \\ \delta_i^{(2)} &= f'\left(\text{net}_i^{(2)}(k)\right) \sum_{l=1}^{3} \delta_l^{(3)} w_{li}^{(3)}(k), \end{aligned} \tag{30}$$

where $f'(\cdot) = (1 - f^2(x))/2$.

4. Simulation Analysis

The time domain response simulations between the energy-regenerative active suspension and the passive suspension are carried out in MATLAB/Simulink so as to examine the improvement effects and calculate the energy regeneration efficiency of the active suspension. Meanwhile, a single PID control simulation is performed to illustrate the improvement of the PID controller combined with the BP algorithm. Also, the three parameters of the fixed gain PID controller are determined through repeated trials and simulations; among them, the proportional coefficient K_p is 500, the integral coefficient K_i is 5, and the differential coefficient K_d is 1. The vehicle runs at a speed of 20 m/s on a B-grade road, and the simulation time is 20 s. The other parameters are listed in Table 1.

As for the control circuit, it is adjusted by the PI controller. Set the proportional coefficient K_p to 3000 and the integral coefficient K_i to 3. Figure 7 is a comparison chart between desired control force and actual control force. We can see the two curves coincide well. The root mean square values of the two curves are 116.88 N and 115.05 N, respectively. The difference is only 1.57%, indicating a good control effect.

Figures 8–10 give the time-domain response of the body acceleration (BA), suspension working space (SWS), and dynamic tire deflection (DTD) of the active suspension using different controllers compared to the passive suspension. It can be seen that the peak values of these performance indicators using the BP-PID controller are reduced most. Among them, the BA decreases most obviously; the SWS and the DTD are reduced to a certain extent. Therefore, the BP-PID controller can improve the vehicle dynamic performance, especially the vehicle ride comfort.

According to Figures 8–10, we calculated the root mean square (RMS) values of suspension performance indicators to quantitatively describe the improvement effects, which are listed in Table 2.

Compared with the passive suspension, the RMS values of the BA, SWS, and DTD are reduced by 46.31%, 16.96%, and 27.55% by using the BP-PID controller, while these data are 28.70%, 14.04%, and 18.37% with the PID controller. That is to say, the BP-PID controller has better improvement effect than the PID controller, and the qualitative calculation is consistent with the analysis.

In addition, we perform more simulations on the C- and D-class roads at the same vehicle speed. The RMS values are listed in Table 3. To make it clear, the improvements of these performance indicators using the BP-PID controller are demonstrated in Figure 11.

Table 1: Simulation parameters.

Parameter	Value
m_b	320 kg
K_s	20000 N/m
K_t	200000 N/m
G_0	64×10^{-6} m^3/cycle
R	10 Ω
m_w	40 kg
C_s	1000 N·s/m
F_0	0.1 Hz
L	0.3 H
φ	90 N/A

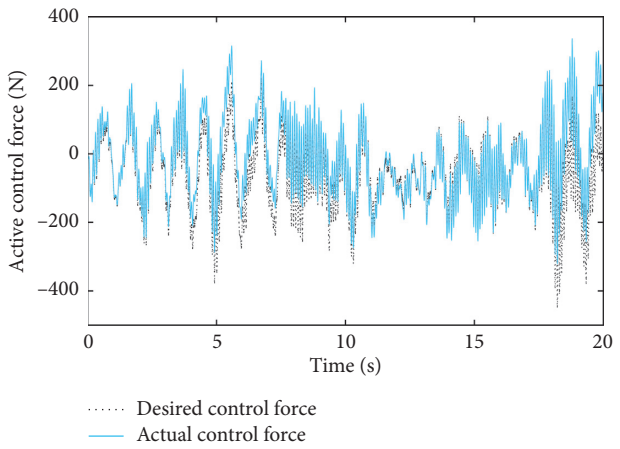

Figure 7: Active control force.

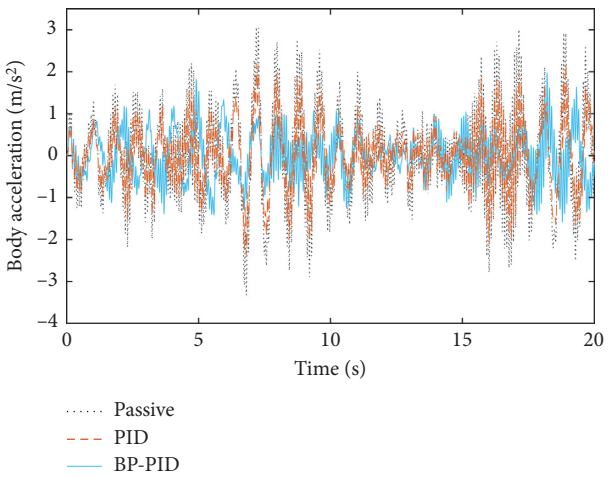

Figure 8: Body acceleration.

According to Table 3 and Figure 11, we can know that these performance indicators are sensitive to the road surface. Compared with the passive suspension, the RMS values of the BA are reduced by 46.31%, 43.52%, and 42.23% under the B-, C-, and D-class roads. For the SWS, these data are 16.96%, 15.54%, and 14.79%. And for the DTD, they are 27.55%, 26.53%, and 25.32%. It can be proved that the control effects decrease slightly when the road surface becomes worse.

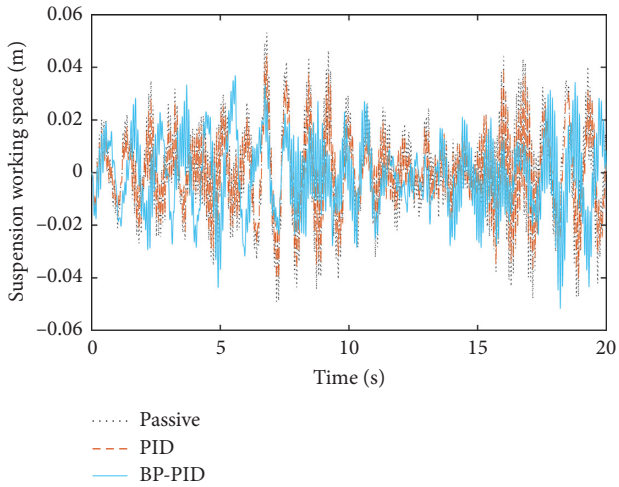

Figure 9: Suspension working space.

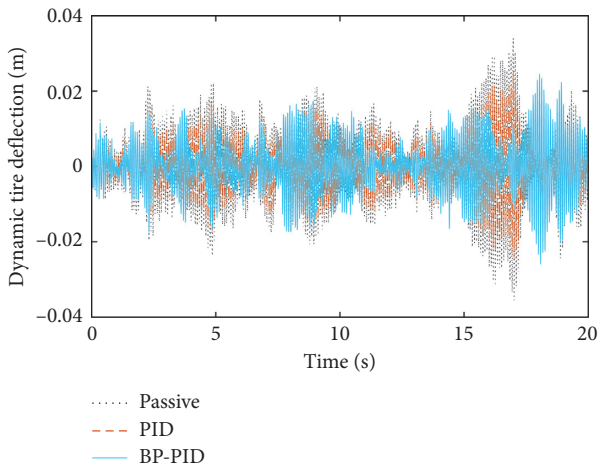

Figure 10: Dynamic tire deflection.

Table 2: RMS values of suspension performance indicators of B-class road.

Performance indicator	BA (m/s^2)	SWS (m)	DTD (m)
Passive	1.0648	0.0171	0.0098
PID	0.7592	0.0147	0.0080
BP-PID	0.5717	0.0142	0.0071

Table 3: RMS values of suspension performance indicators under different roads.

Performance indicator		BA (m/s^2)	SWS (m)	DTD (m)
B-class	Passive	1.0648	0.0171	0.0098
	BP-PID	0.5717	0.0142	0.0071
C-class	Passive	2.1296	0.0341	0.0196
	BP-PID	1.2029	0.0288	0.0144
D-class	Passive	4.2592	0.0683	0.0391
	BP-PID	2.4604	0.0582	0.0292

Furthermore, we perform simulations at different vehicle speeds on the same B-class road. The RMS values are listed in Table 4. Also, the improvements of these

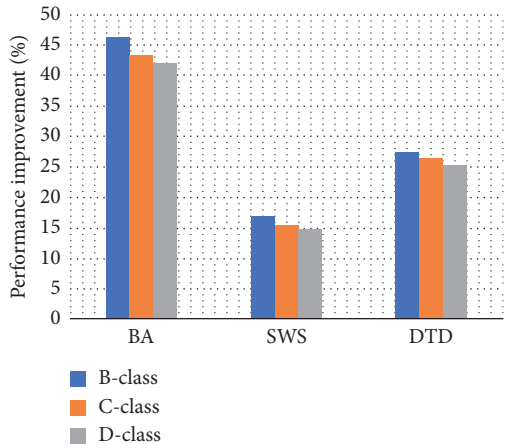

Figure 11: Performance improvement under different roads.

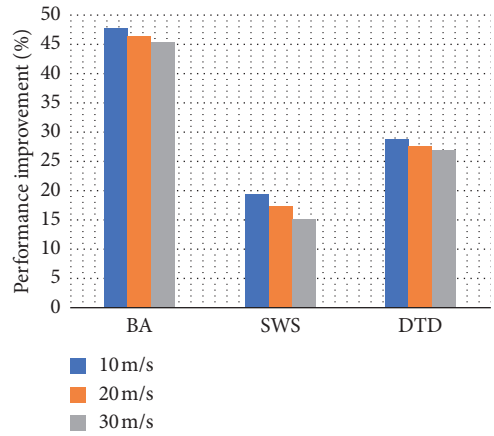

Figure 12: Performance improvement at different vehicle speeds.

Table 4: RMS values of suspension performance indicators at different vehicle speeds.

Performance indicator		BA (m/s^2)	SWS (m)	DTD (m)
10 m/s	Passive	0.7529	0.0121	0.0070
	BP-PID	0.3935	0.0098	0.0050
20 m/s	Passive	1.0648	0.0171	0.0098
	BP-PID	0.5717	0.0142	0.0071
30 m/s	Passive	1.3041	0.0209	0.0120
	BP-PID	0.7131	0.0178	0.0088

performance indicators using the BP-PID controller are demonstrated in Figure 12.

According to Table 4 and Figure 12, we can learn that these performance indicators are also relative with the vehicle speed. Compared with the passive suspension, the RMS values of the BA are reduced by 47.74%, 46.31%, and 45.32% at different vehicle speeds. The RMS values of SWS are reduced by 19.01%, 16.96%, and 14.83%. And for the DTD, they are reduced by 28.57%, 27.55%, and 26.67%. That is to say, the control effects are slightly reduced as the vehicle speed increases.

At last, the self-supply energy efficiency (SSEE) and energy-regenerative efficiency (ERE) of the active suspension with the BP-PID controller are calculated, respectively. The simulation results at the same 20 m/s speed are listed in Table 5. And the calculation data on the same B-class road are listed in Table 6.

According to Tables 5 and 6, we can see that the SSEE is more than 50%, mainly due to the high axial speed of ball screw and the low energy consumption with BP-PID controller. Besides, the SSEE and the ERE are almost constant when the road surface or the vehicle speed is changed. Therefore, it can be proved that the SSEE and the ERE are independent of the input conditions, which include the road surface and the vehicle speed.

In order to study the actual effect of the recovered energy, we take a typical B-class road as an example, and the vehicle is driven at a speed of 72 km/h. Through simulations and calculations, we know that the suspension system can recover 636 kJ of energy per hour, which can be used to increase the mileage of about 1.4 km.

Table 5: Self-supply energy efficiency under different roads.

Road surface	P_r/w	P_c/w	P_d/w	SSEE (%)	ERE (%)
B-class	44.16	79.85	268.13	55.30	16.47
C-class	180.29	324.02	1072.67	55.64	16.81
D-class	719.26	1293.53	4290.69	55.60	16.76

Table 6: Self-supply energy efficiency at different vehicle speeds.

Vehicle speed	P_r/w	P_c/w	P_d/w	SSEE (%)	ERE (%)
10 m/s	21.56	38.92	134.06	55.40	16.08
20 m/s	44.16	79.85	268.13	55.30	16.47
30 m/s	66.01	119.25	402.21	55.35	16.41

5. Conclusions

In this paper, a new energy-regenerative active suspension system is established to achieve active control and vibration energy recovery. The actuator is composed of an energy-regenerative shock absorber and a DC motor. The BP neural network offers the self-adaptive parameters for the PID controller. Also, the control circuit is adjusted by a PI controller. Through simulations, the actual control force coincides with the desired control force well, indicating a good control effect. In addition, the improvement effects of the suspension performances and the system's ability to harvest the suspension vibration energy are verified.

The RMS values of the BA, SWS, and DTD are reduced by more than 40%, 10%, and 20% by using the BP-PID controller, which indicates this system can effectively improve the ride comfort and handing stability of the vehicle, especially the former. In addition, the optimization effects of these performance indicators slightly decrease with the deterioration of the road surface and the increase of the vehicle speed.

A concept of self-supply energy efficiency (SSEE) is proposed to represent the utilization effect of the recovered energy. The SSEE exceeds 50% under different input conditions, mainly due to the high axial speed of ball screw and the low energy consumption with the BP-PID controller. And the energy-regenerative efficiency (ERE) is about 16%. Furthermore, the SSEE and the ERE are almost unchanged

under different road surfaces or vehicle speed input, which indicates the BP-PID controller has good driving condition adaptability and stability.

In future study, the real car experiments will be carried out to further verify the feasibility of this new EERAS system firstly; then, combined with simulations and experiments, the systematic analysis will be conducted to achieve a better or optimal balance between active control and energy regeneration.

Data Availability

The data used to support the findings of this study are included within the article.

Conflicts of Interest

The authors declare that there are no conflicts of interest regarding the publication of this paper.

Acknowledgments

This research is financially supported by the National Natural Science Foundation of China (grant no. 51575288) and the Natural Science Foundation of Shandong Province (grant no. ZR2018BEE020). The authors also express great gratitude to the research team and the editors for their help.

References

[1] A. Alleyne and J. K. Hedrick, "Nonlinear adaptive control of active suspensions," *IEEE Transactions on Control Systems Technology*, vol. 3, no. 1, pp. 94–101, 1995.

[2] D. A. Mantaras and P. Luque, "Ride comfort performance of different active suspension systems," *International Journal of Vehicle Design*, vol. 40, no. 1–3, pp. 106–125, 2006.

[3] S. Nie, Y. Zhuang, W. Liu, and F. Chen, "A semi-active suspension control algorithm for vehicle comprehensive vertical dynamics performance," *Vehicle System Dynamics*, vol. 55, no. 8, pp. 1099–1122, 2017.

[4] P. Hsu, "Power recovery property of electrical active suspension systems," in *Proceedings of the 31st IEEE Energy Conversion Engineering Conference*, vol. 3, pp. 1899–1904, Washington, DC, USA, 1996.

[5] K. Nakano, Y. Suda, M. Yamaguchi, and H. Kohno, "Application of combined type self-powered active suspensions to rubbertired vehicles," *JSAE Annual Congress*, vol. 6, pp. 19–22, 2003.

[6] L. Zuo and P.-S. Zhang, "Energy harvesting, ride comfort, and road handling of regenerative vehicle suspensions," *Journal of Vibration & Acoustics*, vol. 135, no. 1, pp. 1–8, 2013.

[7] M. G. Fodor and R. Redfield, "The variable linear transmission for regenerative damping in vehicle suspension control," *Vehicle System Dynamics*, vol. 22, no. 1, pp. 1–20, 1993.

[8] M. R. Jolly and D. L. Margolis, "Regenerative systems for vibration control," *Journal of Vibration and Acoustics*, vol. 119, no. 2, pp. 208–215, 1997.

[9] B. L. J. Gysen, T. P. J. Van Der Sande, J. J. H. Paulides, and E. A. Lomonova, "Efficiency of a regenerative direct-drive electromagnetic active suspension," *IEEE Transactions on Vehicular Technology*, vol. 60, no. 4, pp. 1384–1393, 2011.

[10] Y. Okada and H. Harada, "Regenerative control of active vibration damper and suspension systems," in *Proceedings of the 35th IEEE Conference on Decision & Control*, vol. 4, no. 1, pp. 4715–4720, Kobe, Japan, 1997.

[11] Y. Okada, H. Harada, and K. Suzuki, "Active and regenerative control of an electrodynamic-type suspension," *JSME International Journal Series C*, vol. 40, no. 2, pp. 272–278, 1997.

[12] Y. Suda, T. Shiiba, K. Hio, Y. Kawamoto, T. Kondo, and H. Yamagata, "Study on electromagnetic damper for automobiles with nonlinear damping force characteristics (road test and theoretical analysis)," *Vehicle System Dynamics*, vol. 41, pp. 637–646, 2004.

[13] K. Nakano, Y. Suda, and S. Nakadai, "Self-powered active vibration control using a single electric actuator," *Journal of Sound and Vibration*, vol. 260, no. 2, pp. 213–235, 2003.

[14] I. Martins, J. Esteves, G. D. Marques, and F. P. daSilva, "Permanent-magnets linear actuators applicability in automobile active suspensions," *IEEE Transactions on Vehicular Technology*, vol. 55, no. 1, pp. 86–94, 2006.

[15] Z. Li, Z. Brindak, and L. Zuo, "Modeling of an electromagnetic vibration energy harvester with motion magnification," *ASME International Mechanical Engineering Congress and Exposition*, vol. 7, pp. 285–293, 2011.

[16] Z. Li, L. Zuo, G. Luhrs, L. Lin, and Y.-X. Qin, "Electromagnetic energy-harvesting shock absorbers: design, modeling, and road tests," *IEEE Transactions on Vehicular Technology*, vol. 62, no. 3, pp. 1065–1074, 2013.

[17] Y. Zhang, X. Zhang, M. Zhan, K. Guo, F. Zhao, and Z. Liu, "Study on a novel hydraulic pumping regenerative suspension for vehicles," *Journal of the Franklin Institute*, vol. 352, no. 2, pp. 485–499, 2015.

[18] D. Ning, S. Sun, H. Du, W. Li, and N. Zhang, "Vibration control of an energy regenerative seat suspension with variable external resistance," *Mechanical Systems and Signal Processing*, vol. 106, pp. 94–113, 2018.

[19] X. H. Shi, H. L. Gao, and M. H. Xu, "Optimization design of automobile suspension springs based on BP," *Applied Mechanics and Materials*, vol. 42, pp. 82–85, 2010.

[20] S.-A. Liu and Q.-Y. Hu, "Application of PSO-BP network algorithm in optimization of automotive suspension," *Journal of Jilin University*, vol. 39, no. 3, pp. 571–575, 2009.

[21] Y.-F. Zhu, Z.-Q. Gu, and S. Zhang, "Mining dump truck's ride comfort optimization based on road surface identification," *Journal of Vibration & Shock*, vol. 34, no. 13, pp. 24–30, 2015.

[22] H. P. Wang, G. I. Y. Mustafa, and Y. Tian, "Model-free fractional-order sliding mode control for an active vehicle suspension system," *Advances in Engineering Software*, vol. 115, pp. 452–461, 2018.

[23] J.-S. Chiou, S.-H. Tsai, and M.-T. Liu, "A PSO-based adaptive fuzzy PID-controllers," *Simulation Modelling Practice and Theory*, vol. 26, pp. 49–59, 2012.

[24] W. Wang, Y. Song, Y. Xue, H. Jin, J. Hou, and M. Zhao, "An optimal vibration control strategy for a vehicle's active suspension based on improved cultural algorithm," *Applied Soft Computing*, vol. 28, pp. 167–174, 2015.